X-ray diffraction evidence for myosin-troponin connections and tropomyosin movement during stretch activation of insect flight muscle

Robert J. Perz-Edwards[a,1], Thomas C. Irving[b], Bruce A. J. Baumann[c], David Gore[b], Daniel C. Hutchinson[a], Uroš Kržič[d], Rebecca L. Porter[a], Andrew B. Ward[e], and Michael K. Reedy[a]

[a]Department of Cell Biology, Box 3011, Duke University, Durham, NC 27710; [b]Biophysics Collaborative Access Team and Department of Biological, Chemical, and Physical Sciences, Illinois Institute of Technology, 3101 South Dearborn, Chicago, IL 60616; [c]Institute of Molecular Biophysics, Florida State University, 91 Chieftan Way, Tallahassee, FL 32306; [d]Cell Biology and Biophysics Unit, European Molecular Biology Laboratory, Meyerhofstrasse 1, 69117 Heidelberg, Germany; and [e]Department of Molecular Biology, The Scripps Research Institute, 10550 North Torrey Pines Road, La Jolla, CA 92037

Edited by James A. Spudich, Stanford University, Stanford, CA, and approved November 5, 2010 (received for review September 28, 2010)

Stretch activation is important in the mechanical properties of vertebrate cardiac muscle and essential to the flight muscles of most insects. Despite decades of investigation, the underlying molecular mechanism of stretch activation is unknown. We investigated the role of recently observed connections between myosin and troponin, called "troponin bridges," by analyzing real-time X-ray diffraction "movies" from sinusoidally stretch-activated *Lethocerus* muscles. Observed changes in X-ray reflections arising from myosin heads, actin filaments, troponin, and tropomyosin were consistent with the hypothesis that troponin bridges are the key agent of mechanical signal transduction. The time-resolved sequence of molecular changes suggests a mechanism for stretch activation, in which troponin bridges mechanically tug tropomyosin aside to relieve tropomyosin's steric blocking of myosin–actin binding. This enables subsequent force production, with cross-bridge targeting further enhanced by stretch-induced lattice compression and thick-filament twisting. Similar linkages may operate in other muscle systems, such as mammalian cardiac muscle, where stretch activation is thought to aid in cardiac ejection.

Stretch activation is a striking example of mechanical signal transduction, in which stretching a partially activated muscle yields, after a delay, greater activation. It is observed to varying degrees in all striated muscles, is prominent in vertebrate cardiac muscle where it may underlie the Frank–Starling relationship (1), and is essential to flight in multiple orders of insects, which together comprise ∼75% of insect species (2) and fully half of all animal taxa (3). Since stretch activation was first reported by Pringle (4), a great deal has been learned about how muscular contraction is driven by cyclic myosin–actin interactions (5) which, in vertebrate skeletal muscles, are controlled by calcium's effect on the steric blocking action of troponin–tropomyosin (6). However, even atomic resolution models of myosin–actin (7) and the troponin complex (8, 9) fail to shed any light on the mechanism of activation by stretch. The central question of stretch activation remains: How does mechanical stress convert to myosin–actin activation while the requisite [Ca^{2+}] stays constant?

Recently we observed cross-bridges between thick (mainly myosin) filaments and thin (mainly actin–troponin–tropomyosin) filaments at the level of the troponin (10). These myosin–troponin connections, referred to here simply as troponin bridges, comprised about 15% of all cross-bridges identified in an insect flight muscle (IFM) quick frozen during an isometric contraction. Troponin bridges represent a newly recognized class of cross-bridges, distinct from the "traditional" force-generating myosin cross-bridges that bind to actin target zones halfway between troponins in IFM (10, 11). The direct observation of troponin bridges revived a previously speculative mechanism for stretch activation (12), in which troponin bridges serve as the agent of mechanical signal transduction by directly linking the myosin thick filaments to the troponin–tropomyosin regulatory system on the thin filament.

It is 40 y since the first synchrotron diffraction from insect muscle was recorded (13). Thanks to that pioneering work and subsequent improvements in synchrotron and X-ray detector technology, we were able to record real-time X-ray diffraction movies of stretch activation. We sought further evidence for the existence and dynamic action of troponin bridges by comparing sinusoidally stretch-activated *Lethocerus* flight muscle to identically stretched-relaxed controls. This allowed us to test our key hypothesis that tropomyosin directly regulates myosin–actin by steric blocking, analogous to vertebrate skeletal muscle regulation, but via stretch-sensitive mechanical connections, presumably troponin bridges.

Results

At physiological temperatures (35–40°), chemically skinned *Lethocerus* IFM gives maximal power at normal wing-beat frequencies (20–40 Hz), but at 20° the stretch activation response is slowed (14, 15). We took advantage of the slower kinetics at 20° and oscillated the muscles at ∼2 Hz, the frequency at which the work per cycle is maximal (Fig. 1). *Lethocerus* IFM also has an extremely well-ordered filament lattice which produces nearly crystalline diffraction patterns (Fig. 2) with individual reflections whose specific correspondence to myosin, actin, troponin, and tropomyosin structures has been well established through combined X-ray diffraction and electron microscopy studies. The X-ray diffraction movies recorded the key changes, some visually obvious (Movie S1), the rest evident by intensity and spacing measurements, averaged from 430 stretch cycles imaged at 32 frames per cycle and synchronized with length and force records.

X-Ray Diffraction Evidence for Troponin Bridges. Actin filaments are not perfectly rigid, and stretching active muscles fractionally elongates the thin filaments (16, 17). Because we also observe troponin bridges in chemically fixed relaxed muscles (Fig. 3), we hypothesized that stretching relaxed muscles might also elongate the thin filaments, which we estimated from three thin-filament-based X-ray reflections. The axial spacings of the sixth and seventh actin layer lines (S_{A6} and S_{A7}, at 5.9 and 5.1 nm, respectively; see Fig. 2) measure the pitch of left- and right-handed helices drawn through the actin monomers of the thin filaments,

Author contributions: R.J.P.-E. designed research; R.J.P.-E., T.C.I., B.A.B., D.G., D.C.H., U.K., R.L.P., A.W., and M.K.R. performed research; R.J.P.-E. analyzed data; D.G. adapted beamline hardware and software; and R.J.P.-E., T.C.I., and M.K.R. wrote the paper.

The authors declare no conflict of interest.

This article is a PNAS Direct Submission.

[1]To whom correspondence should be addressed. E-mail: rjpe@cellbio.duke.edu.

This article contains supporting information online at www.pnas.org/lookup/suppl/doi:10.1073/pnas.1014599107/-/DCSupplemental.

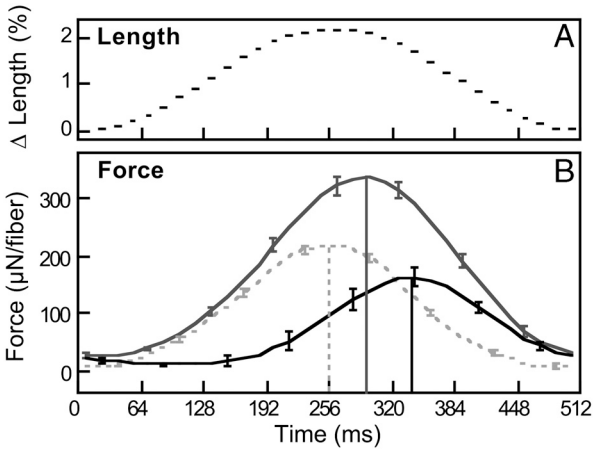

Fig. 1. Stretch activation is marked by tension rise that is delayed relative to the length change. (*A*) Sinusoidal length change (2.2%) imposed on fibers. Normal *Lethocerus* fibers are opaque and sarcomere length is not easily measured, but we estimate the relative sliding to be 16.2 nm/half-sarcomere, based on the results of Linari et al. (39). Horizontal bars indicate 8-ms X-ray exposures taken every 16 ms during the 512-ms-long cycles. (*B*) Force per fiber in response to the length change. Net active force (black) is the total active force (dark gray) minus the passive force (light gray), and represents the force generated by actin-myosin interactions. Note that net active force is delayed, i.e., shifted to the right, relative to the passive force, which peaks in phase with the length change. Vertical lines mark the relative timing of maxima. Data are mean ± SEM; $N = 12$.

whereas the spacing of the troponin reflection (S_{Tn}) measures the axial separation of troponins along the thin filaments. The time courses (Fig. 4*A*) show that all three spacings change together during relaxed length cycling, peaking in phase with the passive

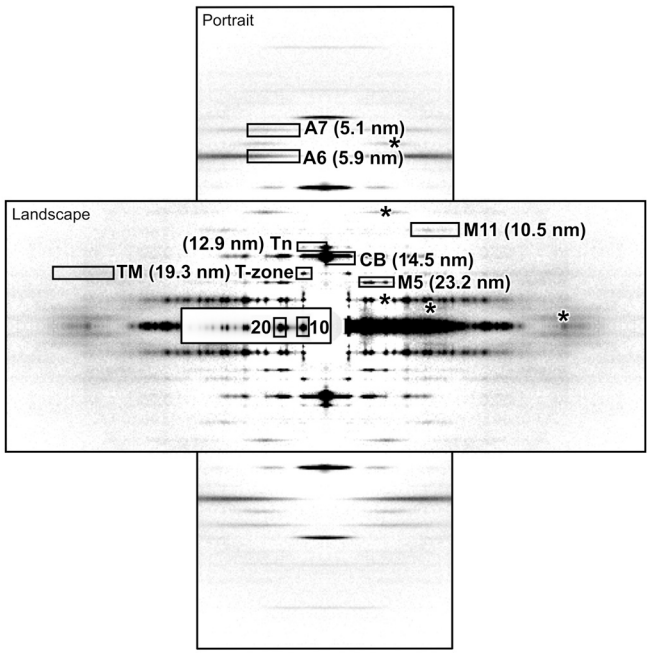

Fig. 2. Sample X-ray diffraction pattern with the 10 major reflections reported here marked. Patterns are symmetric about both the horizontal and vertical axes (called the equator and meridian respectively). Reflections from the thin or thick filaments are marked on the left or right, respectively, with the nominal axial spacing indicated in parentheses. Asterisks mark five additional thick-filament layer lines which are discussed. Inset box on the left side of the equator is displayed at a lower gain to show the equatorial reflections from the hexagonal array of thick and thin filaments. Experiments were done with the detector in two orientations, marked landscape and portrait. See also Movie S1.

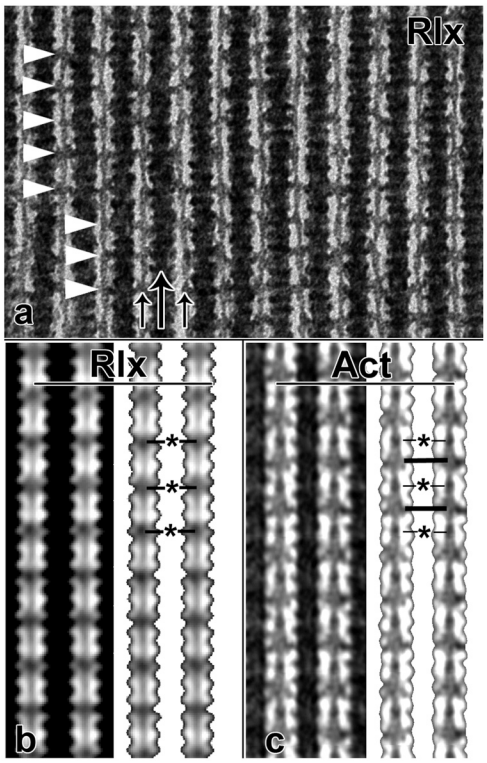

Fig. 3. Myosin-troponin bridges are visible in chemically fixed, relaxed IFM. Electron micrographs (*A*) show periodic cross-bridges (arrowheads) between the thick (large arrow) and thin filaments (small arrows) with an ~39-nm periodicity. These had been observed previously, but were misidentified as precursors of "conventional," stereospecific myosin–actin contacts (50), until the results of Wu et al. (10) forced us to reevaluate them and recognize their position relative to troponin. Computer averaged images clarify the different axial locations of cross-bridges in relaxed (*B*) and active (*C*) muscles. In the right sides of *B* and *C*, the thick filaments have been masked out to highlight the thin filaments, which are marked by a dark "bead" of troponin (asterisks) every 39 nm. In relaxed fibers (*A* and *B*) the predominant cross-bridges connect exactly at the level of the troponins (asterisks with medium bars in *B*). By contrast, in active fibers (*C*) the predominant cross-bridges (heavy bars) connect to actin target zones midway between troponins (10, 11).

force, indicating that the thin filaments are elongated by ~0.09%. To explain thin-filament elongation in relaxed muscle requires some relatively long-lived connections between the thick and thin filaments to transmit force as filaments slide, and in IFM the only candidates for such connections are the troponin bridges observed by EM (10). During stretch activation (Fig. 4*B*), the thin filaments elongate more, by ~0.14%, peaking in phase with the total active force, giving a Young's modulus of 2.4 GPa for the thin filaments, similar to that reported previously for vertebrates (16, 17). There have been conflicting reports concerning whether the thin-filament elongation observed in frog muscle does (17) or does not (16) also involve twisting of the filament. However, because the pitches of the left- and the right-handed actin helices (S_{A6}, S_{A7}) observed here change together and do not diverge, actin elongation in IFM appears not to involve any azimuthal twisting of the actin filaments.

We next examined the cross-bridge (CB) reflection (meridional reflection at 14.5 nm; see Fig. 2), a thick-filament reflection whose intensity (I_{CB}) reports the average angular tilt of myosin heads relative to the thick-filament backbone (18). If troponin bridges exist in an unfixed, relaxed muscle, oscillating the muscle should cause cyclic changes in I_{CB} as the troponin bridges are forced to tilt. As predicted, we observe changes in I_{CB} (Fig. 4*C*, black X), confirming a population of myosin heads that stay attached to the thin filaments, even though there is no free calcium

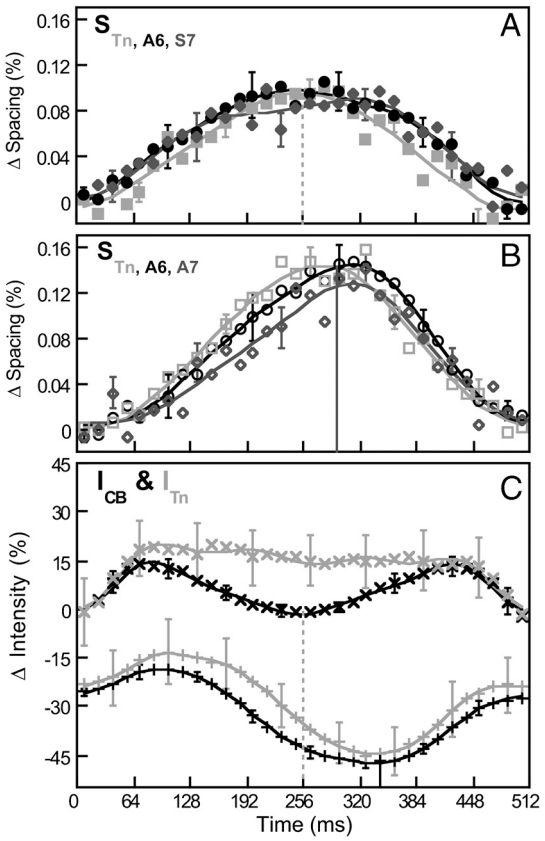

Fig. 4. Relative spacing changes of the Tn, A6, and A7 reflections reveal thin-filament elongation in both in relaxed (*A*, closed symbols) and stretch-activated (*B*, open symbols) muscles. S_{Tn}, light-gray squares; S_{A6}, black circles; S_{A7}, dark-gray diamonds. Vertical lines indicate peak total active (dark gray) and passive (light gray) force, as in Fig. 1*B*. Note that all three reflections change in unison. Compare to Fig. 6*C*. (*C*) Intensities of the cross-bridge reflection (I_{CB}, black) and the troponin refection (I_{Tn}, gray) reveal correlated changes in myosin head and troponin structure. Upper curves (X) are from relaxed fibers; lower curves (+) are from stretch-activated fibers. Note also that the relaxed I_{CB} changes are also very similar to the relaxed I_{TM} changes (Fig. 5*A*, gray X) but of opposite sign. Data are mean ± SEM; $S_{A6,A7}$, $N = 6$; S_{Tn}, $N = 12$.

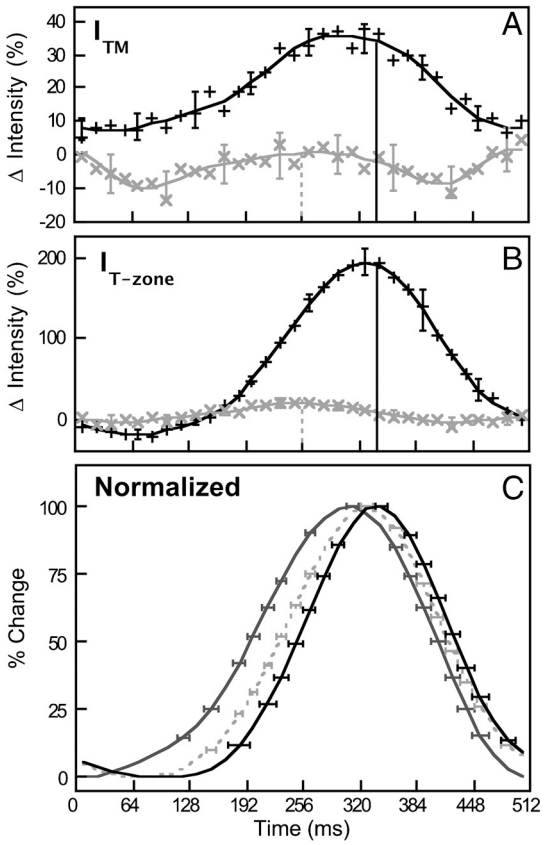

Fig. 5. Stretch activation induces azimuthal movement in tropomyosin followed by myosin binding to actin, in turn followed by active force production. (*A*) Intensity of the tropomyosin reflection (I_{TM}). (*B*) Intensity of the target-zone reflection ($I_{T\text{-}ZONE}$). Peaks in I_{TM} and $I_{T\text{-}ZONE}$ precede the peak in net active force (black vertical lines as in Fig. 1*B*). Stretch activated, black +; stretched-relaxed, gray X. (*C*) Normalized changes highlight the relative timing of events. The black, smoothed curves (see *SI Methods*) from Figs. 5 *A* and *B* and 1*B* are reproduced in Fig. 5*C*, normalized to 100% change. I_{TM} (dark gray) clearly precedes $I_{T\text{-}zone}$ (light gray), which precedes the net active force (black). This is true during both the rising phase and the falling phases. Data are mean ± SEM; I_{TM}, $N = 6$; $I_{T\text{-}ZONE}$, $N = 12$.

present and the fibers are not producing active force. Unexpectedly, the relaxed I_{CB} changes are bimodal, with two symmetric maxima and minima, suggesting that thin-filament sliding pulls the myosin heads back and forth between two opposite tilts (two I_{CB} minima), passing through perpendicular (two I_{CB} maxima) during both stretch and release.

The observed I_{CB} changes during stretch activation (Fig. 4*C*, black +) exactly duplicate previous reports for *Lethocerus* (19). The small initial rise in I_{CB} during stretch activation suggests that troponin bridges are also present during stretch activation and are being tilted back and forth by the filament sliding, as in the relaxed muscle. However, their signal is only observed early in the stretch activation cycle, before the more numerous force-producing cross-bridges bind to actin (see Fig. 5*B*) with widely dispersed tilt angles and come to dominate the I_{CB} signal. We note that the observed I_{CB} change (~45%) is smaller than the 400% change seen in *Drosophila* (20), but the smaller relative change in *Lethocerus* likely represents a genuine species difference. The 14.5-nm reflection is very strong in *Lethocerus*, but is much weaker in *Drosophila* (20), due to a less prominent 14.5-nm periodicity in the thick filaments, and a filament superlattice that makes the 14.5-nm reflection not a true meridional reflection, features that appear unique to Dipterans (21).

Troponin bridges should also impose a strong correlation between myosin structure and troponin structure during both stretch activation and relaxed controls. The troponin reflection (meridional reflection at 12.9 nm in IFM; see Fig. 2) is a thin-filament reflection whose intensity (I_{Tn}) reports conformational changes in the troponin complex on the thin filaments in IFM (22). When I_{Tn} is plotted together with I_{CB}, it reveals a marked correlation (Fig. 4*C*, gray). In the fibers primed for stretch activation (~2 μM free calcium), both intensities start ~25% below their relaxed values and these are the only two reflections which show such a drop relative to the relaxed values. During stretch activation, both I_{CB} and I_{Tn} show an early maximum followed by a subsequent minimum. The only divergence appears during relaxed cycling, when I_{Tn} shows a plateau instead of the central minimum seen in I_{CB}. The simplest explanation for the striking overall similarity between I_{Tn} and I_{CB} is that they are reporting stretch-induced force transmission between myosin and troponin by a physical coupling, i.e., a bridge, consistent with the existence of troponin bridges. Taken together, thin-filament elongation (S_{A6}, S_{A7}, S_{Tn}), myosin tilting (I_{CB}), and troponin structural changes (I_{Tn}) provide strong X-ray diffraction evidence for a linkage between myosin heads and troponin, consistent with the structures observed by EM (10).

Time-Resolved Sequencing of Molecular Changes. Our central hypothesis, that tropomyosin directly regulates myosin–actin interactions during stretch activation, leads to three key predictions. First, we should see evidence that tropomyosin is moving during stretch activation, cyclically allowing and preventing myosin–actin binding. Second, tropomyosin should be in the blocking position in both relaxed (no free Ca^{2+}) and Ca-primed (2 μM free Ca^{2+}) but unstretched muscles. Third and most importantly, the time-resolved sequence of molecular changes during each cycle of stretch and release should recapitulate the sequence which firmly established steric blocking by tropomyosin in vertebrate muscle, namely that tropomyosin moves first, followed by myosin binding to the exposed actin, followed by the subsequent force production by myosin (6). To test these predictions, we examined the tropomyosin reflection (outer part of the 19.3-nm layer line; see Fig. 2) and the target-zone reflection (innermost spot of the 19.3-nm layer line; see Fig. 2) and compared their timing relative to the net active force development.

In vertebrate muscle, the intensity of the tropomyosin reflection (I_{TM}) starts low in relaxed muscle and increases in intensity as tropomyosin moves azimuthally to expose myosin–actin binding sites (6, 23–26). Here in IFM, we find that I_{TM} is clearly rising and falling during stretch activation (Fig. 5*A*, black +), consistent with our first prediction. In contrast, calcium-free oscillation of relaxed muscles (controls) causes smaller changes in I_{TM} (Fig. 5*A*, gray X). Examining Fig. 5*A* at the end points of the cycle, when the fiber is momentarily unstretched, we find that I_{TM} is approximately the same for both active and relaxed oscillations. Therefore priming calcium alone appears to cause little or no tropomyosin movement without stretch, supporting our second prediction.

The target-zone reflection is an IFM-specific thin-filament reflection whose intensity ($I_{T\text{-}zone}$) signals stereospecific myosin binding to actin (11). Fig. 5*B* shows that $I_{T\text{-}zone}$ also rises and falls during stretch activation (black +), whereas relaxed controls show very little change (gray X). Both I_{TM} and $I_{T\text{-}zone}$ reach their maxima well before the peak in net active force, which is marked by the vertical lines. I_{TM} peaks first, ~25 ms before the net active force, whereas $I_{T\text{-}zone}$ peaks ~12 ms before the net active force (Fig. 5*C*). Thus tropomyosin movement occurs first, followed by myosin binding to actin, then followed by force production, which exactly recapitulates the predicted sequence (6) and is similarly strong evidence that steric blocking by tropomyosin regulates myosin–actin interactions during stretch activation. We also note that, during the release phase of active cycles, I_{TM} and $I_{T\text{-}zone}$ drop closely parallel to and slightly ahead of the drop in net active force (Fig. 5*C*), suggesting that releasing the fiber stretch frees tropomyosin to return to its inhibitory position, quickly switching the muscle off.

Passive Structural Changes: Filament Lattice Compression and Myosin Twist. One visually obvious change in the X-ray movies is a side-to-side "breathing" of the patterns, indicating that the thick and thin filaments draw closer together as the fiber is stretched. This lattice compression is a well-known phenomenon in muscle (27). Here we see that our 2.2% fiber stretch causes the thick and thin filaments to move ~0.4 nm closer together, in phase with the length change for both stretch-activated muscles and relaxed controls (Fig. 6*A*). We thus interpret this lattice compression as a passive response to fiber stretch. However, we also note that the interfilament distance in stretch-activated muscles (Fig. 6*A*, black +) is consistently about 0.1 nm smaller than in relaxed controls (Fig. 6*A*, gray X), indicating an additional radial component of cross-bridge force due to active cross-bridges (28, 29).

As the thick and thin filaments draw closer together, the probability of interactions between actin and myosin increases. If the closer proximity between thick and thin filaments also results in movement of the myosin heads away from the thick-filament backbone and toward the thin filament, we would expect to see an increase in the ratio of intensities of the 20 and 10 equatorial reflections (30). We do observe an ~10% increase in I_{20}/I_{10} in relaxed controls and a slightly larger increase in stretch-activated muscles (Fig. 6*B*). Although the relaxed I_{20}/I_{10} showed a maximum approximately centered at 256 ms, i.e., in phase with the length change, the stretch-activated I_{20}/I_{10} shows an additional peak delayed with respect to the length change. The modest changes in I_{20}/I_{10} seen here are consistent with the observations of others (31) and with the small radial movement (2 nm) required for a myosin head to reach actin, as modeled by Al-Khayat et al. (32). The I_{20}/I_{10} rise in relaxed muscle rise

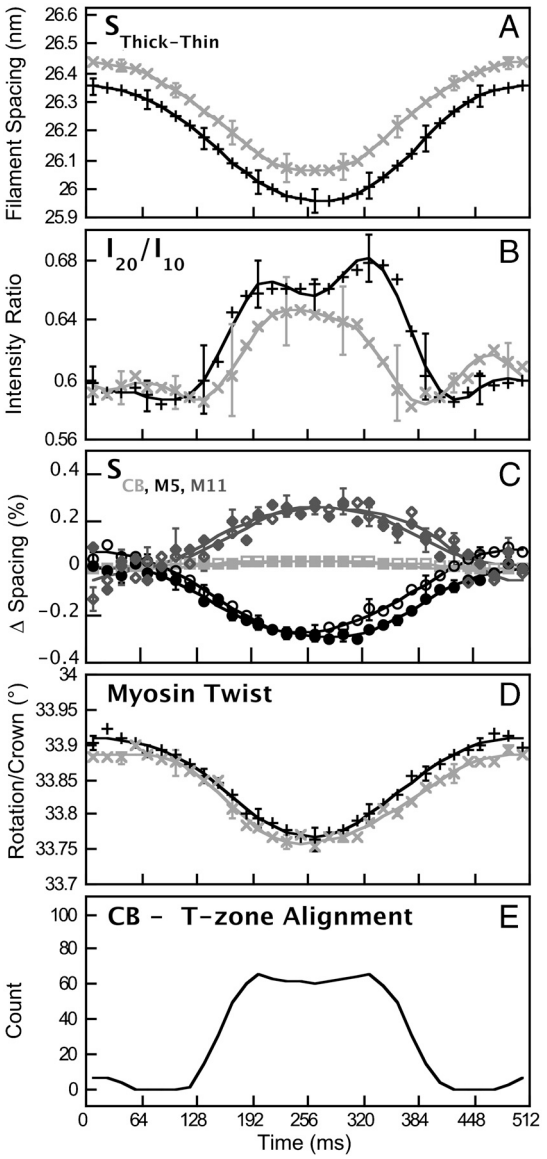

Fig. 6. Fiber stretch passively squeezes filaments closer together and twists the thick filaments. (*A*) Distance between thick- and thin-filament centers in stretch-activated muscles (black +) and stretched-relaxed controls (gray X). (*B*) Intensity ratio of the 20 and 10 equatorial reflections. Symbols as in *A*. (*C*) Relative spacing changes of three thick-filament reflections indicate thick-filament twist in both stretch-activated muscles (open symbols) and stretched-relaxed controls (closed symbols). S_{CB}, light-gray squares; S_{M5}, black circles; S_{M11}, dark-gray diamonds. Compare to Fig. 4 *A* and *B*. See also Fig. S1. (*D*) Derived myosin rotation per crown. Symbols as in *A*. (*A*–*D*) Data are mean ± SEM; $N = 12$. (*E*) Calculated number of matches between target zones and cross-bridges for one-half of a thick filament during stretch activation. See also Movie S2 and Fig. S3.

must be attributable to increased "weak binding cross-bridges" (33) because tropomyosin appears to be in the blocking position (Fig. 5*A*, gray X), whereas the additional I_{20}/I_{10} increase in stretch-activated muscles is presumably due to active force-producing cross-bridges.

A wholly unexpected structural change we observed was myosin filaments twisting as the fibers are stretched. The axial spacings of the 5th and 11th myosin layer lines (S_{M5} and S_{M11}, at 23.2 and 10.5 nm, respectively; see Fig. 2) measure the pitch of left- and right-handed helices drawn through the origins of the myosin heads on the thick filaments, whereas the spacing of the cross-bridge reflection (S_{CB}) measures the axial separation of heads along the thick filament. The cyclic changes in spacing for these three reflections (Fig. 6*C*) imply that oscillation of the fiber length causes the thick filaments to twist so that their left-handed helices are wound tighter and their right-handed helices are unwound as the fiber is stretched. Myosin filament twist is confirmed by changes observed in five additional myosin-based reflections (asterisks in Fig. 2), in which all left-handed helices decrease in spacing and all right-handed helices increase in spacing with fiber stretch (Fig. S1). In addition to twisting, the myosin filaments are also elongating by ~0.05% (Fig. S2). This gives a Young's modulus of 2.7 GPa for IFM thick filaments, slightly larger than, but still consistent with, previous reports for vertebrate thick filaments (16, 17), which have a different helical arrangement of myosin molecules.

Any pair of spacings from the eight myosin reflections can be used to calculate a theoretical twisting for the myosin filaments and all give similar results. We used a least-squares routine to determine the twist that best fit all of the data and found that fiber stretch caused successive "crowns" of myosin heads, which are separated by 14.5 nm axially, to rotate ~0.15° relative to one another (Fig. 6*D*). Assuming this 0.15° relative twist is cumulative over the ~80 crowns in each half of the bipolar thick filament implies ~12° of twist (clockwise, viewed from the Z band) at the ends of the thick filament relative to the center, or twice that from end to end. The twist is similar in stretch activation and the relaxed controls and is approximately in phase with the fiber length, not tension. Therefore, myosin filament twist appears to be a passive response to fiber stretch.

We reasoned that the cumulative myosin twist would imply that the myosin heads nearest the middle of the sarcomere, where the twist is smallest, would "see" a very different arrangement of actin target zones than would the myosin heads at the end of the thick filament, where the twist has rotated the myosin head origins ~12°. We therefore evaluated the alignment between the helical array of cross-bridges on one-half of the bipolar thick filament and the surrounding helix of target zones on the six nearest thin filaments. We counted the number of cross-bridges within reach of an actin target zone for each frame of our X-ray movie, first assuming the cross-bridges could reach ±9 nm axially and ±12° azimuthally, and then incorporating our dynamic spacing data for the thick- and thin-filament elongation, the deduced thick-filament twist, and the relative filament sliding. The time-varying alignment between cross-bridges and target-zones is shown visually in Movie S2 and is scored in Fig. 6*E*. The exact shape for the cross-bridge–target-zone alignment shown in Fig. 6*E* depends on the assumed reach of the cross-bridges and the initial offset between cross-bridges and target zones, but the general shape is similar when other assumptions were explored (see Fig. S3) and bears a striking resemblance to the observed I_{20}/I_{10} changes (Fig. 6*B*).

Discussion

Proposed mechanisms for the 60-y mystery of stretch activation have included helical matching between thick and thin filaments (34, 35), lattice spacing changes (36), stress-induced changes in myosin activity (14, 37–39), and stress-induced changes in thin-filament activation (12, 40–42). We favor the last mechanism, and our results, particularly the time-resolved sequence of tropomyosin movement, cross-bridge binding and force production, strongly support the hypothesis that steric blocking–unblocking by tropomyosin regulates stretch activation. We have also presented strong X-ray diffraction evidence for the existence of strain-bearing structures at the level of the troponins, consistent with the structures originally observed by EM (10). Although we have not provided direct evidence that troponin bridges mediate the movement of tropomyosin, they are at present the only obvious candidates to do so. Our working model is that troponin bridges mechanically tug tropomyosin aside as the fiber is stretched. Such a direct coupling between myosin and the troponin–tropomyosin regulatory system would provide the insect with an intrinsic and automatic way of activating and relaxing its flight muscles with every wing beat, regardless of frequency, and could easily accommodate the high wing-beat frequency of some insects (~1,000 Hz; ref. 43), provided they also evolved a fast enough myosin (44) to make use of the rapidly oscillating tropomyosin movement (42).

Oscillations of relaxed muscles highlight the permissive but essential role of calcium in stretch activation. In the absence of calcium, length oscillations drive only a restricted motion of the myosin–troponin–tropomyosin linkages, as shown by the small changes in relaxed I_{TM}, $I_{T\text{-}zone}$, I_{Tn}, and I_{CB}. To offer an analogy, relaxed oscillations are shaking the gate (tropomyosin) but unable to open it without calcium to unlock the gate. On the other hand, adding calcium to the priming level unlocks the gate but leaves it shut, until fiber stretch tugs the gate open via myosin–troponin bridges. In this analogy, the lock must be F1-troponin C, which is the calcium binding protein associated with stretch activation in *Lethocerus* (40). With only a single functional calcium binding site in the C-terminal lobe, F1-troponin C is still poorly understood. However, its 93% occupancy by calcium ($K_D = 0.16$ μM; ref. 40) in our stretch activation solutions makes it the obvious candidate for mediating the permissive role of calcium.

Our results can reconcile previous results that led to alternative proposals for the mechanism of stretch activation. Our finding that thick filaments twist with stretch, causing more myosin heads to become aligned with the actin target zones is reminiscent of the helical "match-mismatch" model (34). Similarly, our finding that the filament lattice compresses with stretch is reminiscent of the lattice spacing model (36). Both of these changes occur during stretch activation, but it is unlikely that they are regulating myosin–actin interactions per se, because they likewise occur in relaxed muscles, where the myosin heads are unable to take full advantage of their fleeting alignment with and approach to target zones due to steric blocking by tropomyosin, except perhaps as weak binding bridges as suggested by the changes in I_{20}/I_{10} (Fig. 6*B*, gray X). These effects may, however, modulate the stretch activation response and help explain why the stretch activation response is stronger in IFM than any other muscle type. The elastic filaments projectin and kettin (45) probably supply the radial force for lattice compression and if they bind tangentially to the end of the thick filament could also supply the necessary torque for myosin filament twist. This could explain the loss of flight in heterozygous kettin mutants in *Drosophila* (46).

Our model of troponin bridges, which mechanically tug tropomyosin aside, provides a testable molecular mechanism for stretch activation. Stretch activation is observed to varying degrees in a wide variety of striated muscles (14), especially mammalian cardiac muscle (1, 47). A similar mechanism may underlie the Frank–Starling relationship, where cardiac muscles develop more force for a given calcium concentration when stretched (length-dependent activation). Because the molecular mechanism for cardiac length-dependent activation remains controversial (48), it

appears worthwhile to seek evidence for troponin bridges in cardiac and other muscles types. To that end, recent resonance energy transfer measurements indicate a close proximity between myosin and troponin in vertebrate skeletal muscle myofibrils (49), consistent with the presence of troponin bridges.

Methods

Twelve detergent-skinned bundles of 20–30 flight muscle fibers were taken from five specimens of *Lethocerus indicus*. Bundles were mounted in a mechanics–X-ray cell described previously (11). X-ray diffraction movies (62.5-Hz frame rate, 8-ms exposure per frame) were collected using the small-angle diffraction instrument on the Biophysics Collaborative Access Team beamline 18 ID at the Advanced Photon Source, Argonne National Laboratory with a PILATUS 100K detector (Dectris. Inc.). Experiments were coordinated by custom LabVIEW (National Instruments) routines that controlled solution flow, fiber length, X-ray shutters, and detector, while recording fiber length, force, and X-ray intensity (1 kHz sampling). Initially, fiber length was adjusted by stretching ~1% in relaxing solution (no added Ca^{2+}) to give ~30 μN/fiber passive force. Fiber length was then sinusoidally stretched 2.2% above this length with a period of 512 ms (1.95 Hz). Two experimental conditions were examined: stretch activation in which the muscle was immersed in activating solution (~2 μM free Ca^{2+}) during the length oscillation, and relaxed cycles in which the muscle was immersed in relaxing solution during oscillation. The X-ray movies covered 16–20 oscillations, which were averaged together to give a single-cycle, 32-frame X-ray movie for each bundle (24 movies total). Each frame of each movie was then analyzed to measure the intensity and spacing of the diffraction spots of interest. Data from relaxed or stretch-activated muscles were averaged together and displayed as a time course for a single length cycle, with 32 points per cycle. Where expressed as a percent change, data were normalized to the relaxed, unstretched value (derived from a three-point average around the first time point). Error bars (SEM) are shown for every fourth or sixth point ($N = 6–12$). More detailed methods are available in the *SI Text*.

ACKNOWLEDGMENTS. Thanks to C. Lucaveche, S. Hester, T Bekyarova, and R.T. Tregear. Muscle data acquisition modules were written by Katya Prince (Prince Consulting LLC, Durham, NC). This research was supported by National Institutes of Health (NIH) Grants AR-14317 (to M.K.R.) and GM-30598 (to B.A.B.). The Advanced Photon Source was supported by the US Department of Energy Contract W-31-109-ENG-38. Biophysics Collaborative Access Team is an NIH-supported Research Center RR-08630.

1. Stelzer JE, Moss RL (2006) Contributions of stretch activation to length-dependent contraction in murine myocardium. *J Gen Physiol* 128:461–471.
2. Josephson RK, Malamud JG, Stokes DR (2000) Asynchronous muscle: A primer. *J Exp Biol* 203:2713–2722.
3. Wheeler QD (1990) Insect diversity and cladistic constraints. *Ann Entomol Soc Am* 83:1031–1047.
4. Pringle JWS (1949) The excitation and contraction of the flight muscles of insects. *J Physiol* 108:226–232.
5. Huxley HE (1969) The mechanism of muscular contraction. *Science* 164:1356–1365.
6. Kress M, Huxley HE, Faruqi AR, Hendrix J (1986) Structural changes during activation of frog muscle studied by time-resolved X-ray diffraction. *J Mol Biol* 188:325–342.
7. Rayment I, et al. (1993) Structure of the actin-myosin complex and its implications for muscle contraction. *Science* 261:58–65.
8. Takeda S, Yamashita A, Maeda K, Maeda Y (2003) Structure of the core domain of human cardiac troponin in the Ca^{2+}-saturated form. *Nature* 424:35–41.
9. Vinogradova MV, et al. (2005) Ca^{2+}-regulated structural changes in troponin. *Proc Natl Acad Sci USA* 102:5038–5043.
10. Wu S, et al. (2010) Electron tomography of cryofixed, isometrically contracting insect flight muscle reveals novel actin-myosin interactions. *PLoS One* 5:e12643.
11. Tregear RT, et al. (1998) X-ray diffraction indicates that active cross-bridges bind to actin target zones in insect flight muscle. *Biophys J* 74:1439–1451.
12. Reedy MC, Reedy MK, Leonard KR, Bullard B (1994) Gold/Fab immuno electron microscopy localization of troponin H and troponin T in *Lethocerus* flight-muscle. *J Mol Biol* 239:52–67.
13. Rosenbaum G, Holmes KC, Witz J (1971) Synchrotron radiation as a source for X-ray diffraction. *Nature* 230:434–437.
14. Pringle JW (1978) The Croonian Lecture, 1977. Stretch activation of muscle: Function and mechanism. *Proc Roy Soc Lond B Biol Sci* 201:107–130.
15. Schadler M, Steiger GJ, Ruegg JC (1971) Mechanical activation and isometric oscillation in insect fibrillar muscle. *Pflug Arch Eur J Phy* 330:217–229.
16. Huxley HE, Stewart A, Sosa H, Irving T (1994) X-ray diffraction measurements of the extensibility of actin and myosin filaments in contracting muscle. *Biophys J* 67:2411–2421.
17. Wakabayashi K, et al. (1994) X-ray diffraction evidence for the extensibility of actin and myosin filaments during muscle contraction. *Biophys J* 67:2422–2435.
18. Irving M, Lombardi V, Piazzesi G, Ferenczi MA (1992) Myosin head movements are synchronous with the elementary force-generating process in muscle. *Nature* 357:156–158.
19. Tregear RT, Miller A (1969) Evidence of crossbridge movement during contraction of insect flight muscle. *Nature* 222:1184–1185.
20. Dickinson M, et al. (2005) Molecular dynamics of cyclically contracting insect flight muscle in vivo. *Nature* 433:330–334.
21. Squire JM, et al. (2006) The myosin filament superlattice in the flight muscles of flies: A-band lattice optimisation for stretch-activation? *J Mol Biol* 361:823–838.
22. Maeda Y (1979) X-ray diffraction patterns from molecular arrangements with 38-nm periodicities around muscle thin filaments. *Nature* 277:670–672.
23. Huxley HE (1973) Structural changes in actin-containing and myosin-containing filaments during contraction. *Cold Spring Harbor Symp Quant Biol* 37:361–376.
24. Haselgrove JC (1973) X-Ray evidence for a conformational change in actin-containing filaments of vertebrate striated-muscle. *Cold Spring Harbor Symp Quant Biol* 37:341–352.
25. Parry DA, Squire JM (1973) Structural role of tropomyosin in muscle regulation: Analysis of the X-ray diffraction patterns from relaxed and contracting muscles. *J Mol Biol* 75:33–55.
26. Poole KJ, et al. (2006) A comparison of muscle thin filament models obtained from electron microscopy reconstructions and low-angle X-ray fibre diagrams from non-overlap muscle. *J Struct Biol* 155:273–284.
27. Elliott GF, Lowy J, Worthington CR (1963) An X-ray and light-diffraction study of filament lattice of striated muscle in living state and in rigor. *J Mol Biol* 6:295–305.
28. Brenner B, Yu LC (1991) Characterization of radial force and radial stiffness in Ca^{2+}-activated skinned fibres of the rabbit psoas muscle. *J Physiol* 441:703–718.
29. Hoskins BK, Ashley CC, Rapp G, Griffiths PJ (2001) Time-resolved X-ray diffraction by skinned skeletal muscle fibers during activation and shortening. *Biophys J* 80:398–414.
30. Worthington CR (1961) X-ray diffraction studies on large-scale molecular structure of insect muscle. *J Mol Biol* 3:618–633.
31. Rapp G, Guth K, Maeda Y, Poole KJ, Goody RS (1991) Time-resolved X-ray diffraction studies on stretch-activated insect flight muscle. *J Muscle Res Cell Motil* 12:208–215.
32. Al-Khayat HA, Hudson L, Reedy MK, Irving TC, Squire JM (2003) Myosin head configuration in relaxed insect flight muscle: X-ray modeled resting cross-bridges in a pre-powerstroke state are poised for actin binding. *Biophys J* 85:1063–1079.
33. Brenner B, Schoenberg M, Chalovich JM, Greene LE, Eisenberg E (1982) Evidence for cross-bridge attachment in relaxed muscle at low ionic strength. *Proc Natl Acad Sci USA* 79:7288–7291.
34. Wray JS (1979) Filament geometry and the activation of insect flight muscles. *Nature* 280:325–326.
35. Abbott RH, Cage PE (1984) A possible mechanism of length activation in insect fibrillar flight muscle. *J Muscle Res Cell Motil* 5:387–397.
36. Garamvölgyi N (1972) Forces acting between muscle filaments. 1. Filament lattice spacing in bee flight muscle. *Acta Biochim Biophys Acad Sci Hung* 7:157–164.
37. Thorson J, White DCS (1969) Distributed representations for actin-myosin interaction in oscillatory contraction of muscle. *Biophys J* 9:360–390.
38. Granzier HL, Wang K (1993) Interplay between passive tension and strong and weak binding cross-bridges in insect indirect flight muscle. A functional dissection by gelsolin-mediated thin filament removal. *J Gen Physiol* 101:235–270.
39. Linari M, Reedy MK, Reedy MC, Lombardi V, Piazzesi G (2004) Ca-activation and stretch-activation in insect flight muscle. *Biophys J* 87:1101–1111.
40. Agianian B, et al. (2004) A troponin switch that regulates muscle contraction by stretch instead of calcium. *EMBO J* 23:772–779.
41. Bekyarova TI, et al. (2008) Reverse actin sliding triggers strong myosin binding that moves tropomyosin. *Proc Natl Acad Sci USA* 105:10372–10377.
42. Iwamoto H, Inoue K, Yagi N (2010) Fast X-ray recordings reveal dynamic action of contractile and regulatory proteins in stretch-activated insect flight muscle. *Biophys J* 99:184–192.
43. Sotavalta O (1952) Flight-tone and wing-stroke frequency of insects and the dynamics of insect flight. *Nature* 170:1057–1058.
44. Swank DM, Vishnudas VK, Maughan DW (2006) An exceptionally fast actomyosin reaction powers insect flight muscle. *Proc Natl Acad Sci USA* 103:17543–17547.
45. Bullard B, Burkart C, Labeit S, Leonard K (2005) The function of elastic proteins in the oscillatory contraction of insect flight muscle. *J Muscle Res Cell Motil* 26:479–485.
46. Hakeda S, Endo S, Saigo K (2000) Requirements of Kettin, a giant muscle protein highly conserved in overall structure in evolution, for normal muscle function, viability, and flight activity of Drosophila. *J Cell Biol* 148:101–114.
47. Vemuri R, et al. (1999) The stretch-activation response may be critical to the proper functioning of the mammalian heart. *Proc Natl Acad Sci USA* 96:1048–1053.
48. de Tombe PP, et al. (2010) Myofilament length dependent activation. *J Mol Cell Cardiol* 48:851–858.
49. Patel DA, Root DD (2009) Close proximity of myosin loop 3 to troponin determined by triangulation of resonance energy transfer distance measurements. *Biochemistry* 48:357–369.
50. Schmitz H, Lucaveche C, Reedy MK, Taylor KA (1994) Oblique section 3-D reconstruction of relaxed insect flight muscle reveals the cross-bridge lattice in helical registration. *Biophys J* 67:1620–1633.

Supporting Information

Perz-Edwards et al. 10.1073/pnas.1014599107

SI Methods

X-Ray Diffraction. We acquired X-ray diffraction movies using the small-angle diffraction instrument on the Biophysics Collaborative Access Team beamline 18 ID at the Advanced Photon Source, Argonne National Laboratory (1), with a 1.3-m sample-to-detector distance. The X-ray beam contained $\sim 10^{13}$ photons per second incident flux at 12 keV beam energy, collimated and focused to $\sim 40 \times 150$ μm at the detector. X-ray patterns were recorded using a PILATUS 100K detector (Dectris, Inc.) with 8-ms exposures recorded every 16 ms. Half of the experiments were done with the long axis of the detector perpendicular to the muscle fiber axis (landscape) to record the tropomyosin reflection, and half were done with the long axis parallel to the fiber axis (portrait) to record the 5.1- and 5.9-nm actin layer lines. The sample stage was attached to a motor driven $X - Y$ slide assembly that rastered the sample across the X-ray beam during exposure to distribute radiation exposure evenly. The raster speed was adjusted so that every point in the fiber received ~100-ms exposure during a single movie. The X-ray beam intensity was monitored using a silicon PIN diode so that open shutter times (exposures) could be recorded and correlated to the force and length data.

Preparations and Data Acquisition. Dorsal longitudinal muscles from *Lethocerus indicus* were detergent skinned as previously described (2). Bundles with 20–30 muscle fibers each were mounted in a mechanics–X-ray cell described previously (3), which allowed temperature control, continuous-flow perfusion, remote control of muscle length and perfusion buffer, and simultaneous force measurement. Relaxing solution contained (in millimolar) 15 Mg acetate, 15 Na_2ATP, 5 EGTA, 20 MOPS, 5 NaN_3, 10 NaCl, pH 6.8. Stretch activation solution was identical but with only 3 NaCl and additionally 3.5 $CaCl_2$, with a free $[Ca^{2+}]$ of ~2 μM (http://www.stanford.edu/~cpatton/CaMgATPEGTA-NIST-Plot.htm). Fiber length and force, chamber temperature, and beam intensity were digitally sampled at 1 kHz and recorded with a custom LabVIEW (National Instruments) data acquisition routine that also controlled the fiber length and timing of the X-ray detector and shutters.

Twelve separate muscle bundles from five different bugs were examined. Initially, each muscle was stretched ~1% in relaxing solution to a base length that gave 30 μN/fiber passive force. The muscle was then perfused with either relaxing or stretch activation solution and sinusoidally stretched 2.2% above the base length for 16–20 cycles with a period of 512 ms (1.95 Hz) while recording a continuous X-ray movie (32 frames per cycle). After the first movie was recorded, the muscle was switched to the alternate solution and a second oscillation movie was recorded. Experiments alternated whether the first movie was recorded in stretch activation or relaxing solution. The 24 movies recorded consisted of 13,760 individual X-ray patterns.

Data Analysis. All data analysis was done using custom written LabVIEW routines (available on request). Individual patterns were centered and rotated to align their axes with the detector axes and normalized to a mean intensity of 10 photons per pixel, excluding the center region up to a radius of 0.039 nm^{-1}. Each movie was then reduced to a single cycle by averaging together corresponding frames from each of its 16–20 cycles. This improved the signal-to-noise ratio and reduced our dataset to 768 individual patterns to be analyzed.

The axial spacings and intensities of all reflections (except tropomyosin reflection, see below) were obtained by integrating in the equatorial direction and peak fitting the resultant 1D projection onto the meridional axis. Equatorial integration limits for each reflection were as follows. Target zone (T zone), 0.013–0.031 nm^{-1}; cross-bridge (CB) and troponin (Tn), 0–0.027 nm^{-1}; actin helix A6 and A7, 0.013–0.065 nm^{-1}; myosin helix M5, 0.034–0.073 nm^{-1}; M11, 0.086–0.125 nm^{-1}. Peak fitting used the Levenberg–Marquardt algorithm with a double exponential function for the diffuse background and a pseudo-Voigtian shape for the diffraction peaks.

The weak tropomyosin reflection could not be fit reliably in all frames by this method, so its intensity was estimated from background-subtracted patterns by integrating within the rectangular region defined by 0.210–0.269 nm^{-1} in the equatorial direction and 0.048–0.060 nm^{-1} in the meridional direction. Background subtraction of each pattern was done by extracting the intensity profile along a center-to-corner diagonal line, which missed all major reflections, except where it crossed the 38.7-nm layer line, and was therefore taken as an estimate of the diffuse background scattering. The 1D intensity profile was fit with a double exponential function, excluding the 38.7-nm layer line region from the fitting, and the fit function for each pattern was subtracted from the 2D pattern by assuming circular symmetry.

Data for corresponding time points from each experimental group (stretch-activated or relaxed) were averaged together and displayed as a time course for a single length cycle with 32 points per cycle. Where results are presented as percent change, data are normalized relative to the un-stretched-relaxed value as derived from a three-point average around the first data point. Error bars for all measurements are drawn for every fourth or sixth data point and represent the standard error of the mean. The number of measurements for each reflection is as follows. Tropomyosin (TM) (visible in landscape patterns), $N = 6$. A6 and A7 reflections (visible in portrait patterns), $N = 6$. T-zone, M5, and M11 reflections (visible in both), $N = 12$. CB and Tn reflections (visible in both, but see following), $N = 6$. The CB reflection was previously known to decrease in intensity due to radiation damage (4), and we likewise found a ~50% decrease in I_{CB} and I_{Tn} in relaxed patterns when comparing first exposure movies (100 ms total exposure) to second exposure movies (200 ms total exposure). Therefore the data from second exposure movies were discarded for the CB and Tn reflections. Other reflections showed no significant effects of radiation damage and so results were pooled from the first and second exposure movies. The smooth lines drawn through the data points were derived by expressing the data as a discrete Fourier series and summing the first four terms. These smooth curves have well defined maxima and minima, and were therefore used to estimate the relative timing of intensity, spacing, and force changes.

Electron Microscopy. Electron micrographs and filtered images were prepared as described previously for relaxed (5) and active (6) muscles.

1. Fischetti R, et al. (2004) The BioCAT undulator beamline 18ID: A facility for biological non-crystalline diffraction and X-ray absorption spectroscopy at the Advanced Photon Source. *J Synchrotron Radiat* 11:399–405.
2. Taylor KA, Wu S, Reedy MC, Reedy MK (2007) Imaging actomyosin in situ. *Methods Cell Biol* 79:321–368.
3. Tregear RT, et al. (1998) X-ray diffraction indicates that active cross-bridges bind to actin target zones in insect flight muscle. *Biophys J* 74:1439–1451.

4. Bekyarova TI, et al. (2007) Effects of dose rate, cooling and freezing on synchrotron X-ray diffraction patterns from relaxed lethocerus insect flight muscle (IFM). 2007 Biophysical Society Meeting Abstracts. *Biophys J* (Suppl) 297a.
5. Schmitz H, Lucaveche C, Reedy MK, Taylor KA (1994) Oblique section 3-D reconstruction of relaxed insect flight muscle reveals the cross-bridge lattice in helical registration. *Biophys J* 67:1620–1633.
6. Taylor KA, et al. (1999) Tomographic 3D reconstruction of quick-frozen, Ca^{2+}-activated contracting insect flight muscle. *Cell* 99:421–431.
7. Pringle JW (1978) The Croonian Lecture, 1977. Stretch activation of muscle: Function and mechanism. *Proc Roy Soc Lond B Biol Sci* 201:107–130.
8. Al-Khayat HA, Hudson L, Reedy MK, Irving TC, Squire JM (2003) Myosin head configuration in relaxed insect flight muscle: X-ray modeled resting cross-bridges in a pre-powerstroke state are poised for actin binding. *Biophys J* 85:1063–1079.

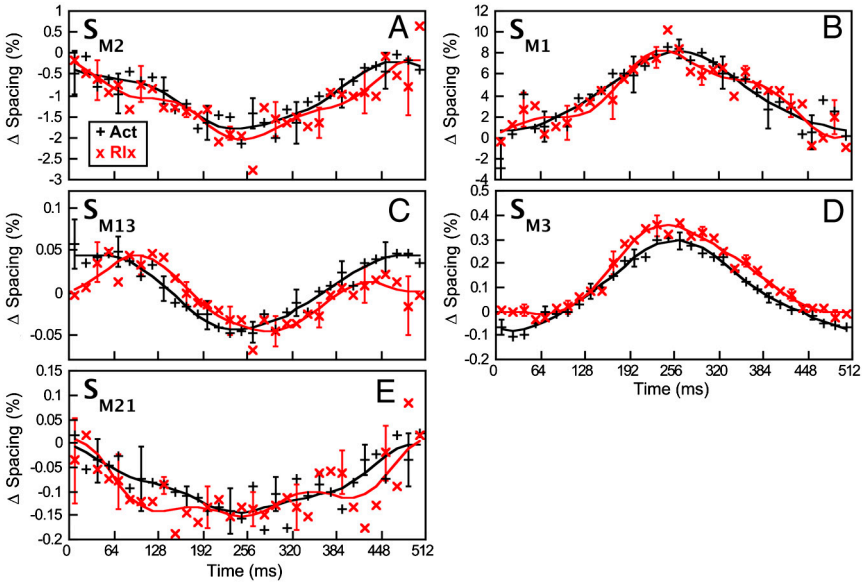

Fig. S1. Spacing changes from all observed myosin layer lines support myosin filament twist. (*A–E*) Spacing changes for the five reflections marked with asterisks in Fig. 2. Layer lines M2, M13, and M21 (*A*, *C*, and *E*) come from left-handed helices and all show a decrease with stretch. Layer lines M1 and M3 (*B* and *D*) come from right-handed helices and both show an increase with stretch. Note that here M3 refers to the third myosin layer line at 38.7 nm in insect flight muscle (IFM) and is not to be confused with the third meridional reflection (at ~14.5 nm, also called "M3") seen in vertebrates X-ray patterns. In this work, we refer to the meridional reflection at 14.5 nm in IFM as the cross-bridge reflection (CB).

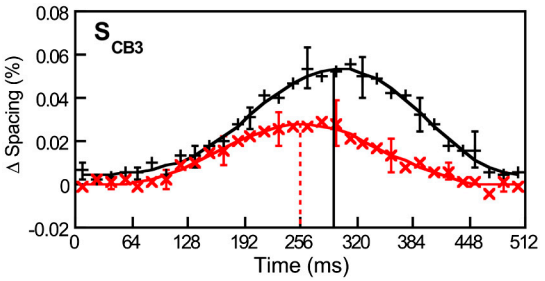

Fig. S2. Myosin filaments elongate as well as twist. Filament elongation is estimated from the spacing of the meridional reflection at 4.8 nm (S_{CB3}), which is the third order of the cross-bridge reflection at 14.5 nm (see Fig. 2). Filaments elongate by ~0.03% in stretched-relaxed muscles (lower curve, red X), and by ~0.05% in stretch-activated muscles (upper curve, black +). Like the actin filament elongation (Fig. 4 *A* and *B*), the myosin filament elongation seen here is approximately in phase with and proportional to the passive or total active force (vertical lines as in Fig. 1). Assuming 338 μN/fiber, 6.7×10^5 thick filaments per fiber (7), and 22-nm-diameter filaments (8), a 0.05% elongation gives a Young's modulus of 2.7 GPa for the thick filaments. Data are mean ± SEM; $N = 6$.

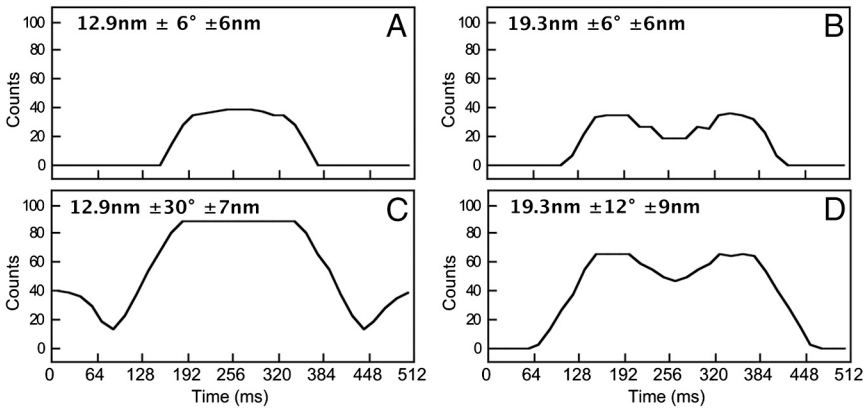

Fig. S3. Calculated number of matches between target zones and cross-bridges for one-half of a thick filament, with varying initial parameters. The numbers at the top of each graph indicate the initial offset between the first crown of cross-bridges and the first target zone, the azimuthal reach of the cross-bridge, and the axial reach of the cross-bridge, respectively. The actual range for these parameters is not known in insect flight muscle, but we examined a plausible range based on the geometry of the filament lattice and known molecular dimensions. Qualitatively, the traces are similar and are roughly symmetric about the center (at 256 ms), due to the symmetry of the myosin filament twist (see Fig. 6*D*). Larger numbers for the axial and azimuthal reach yield a greater number of matches between target zones and cross-bridges (compare *C* and *D* to *A* and *B*). An initial offset of 12.9 nm (*A* and *C*) gives a match that is relatively flat at the center of the stretch-release cycle, whereas an initial offset of 19.3 nm (*B* and *D*) gives a central minimum, indicating that the maximum match occurs with less filament sliding than the imposed 2.2% fiber stretch.

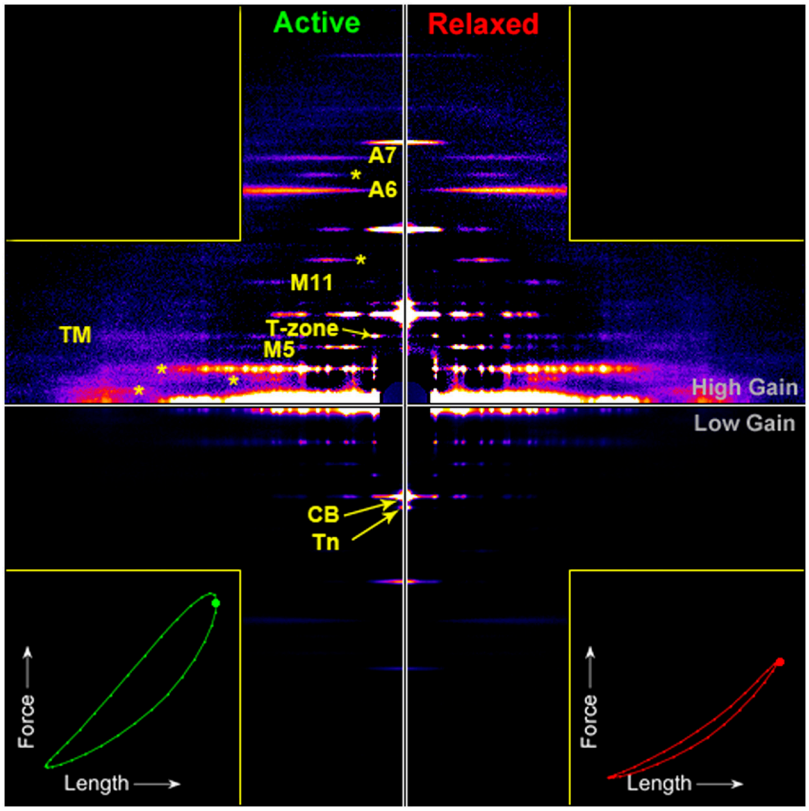

Movie 1. X-ray diffraction movies reveal passive and active structural changes during both stretch activation and relaxed muscle length oscillation. The movie, slowed to about one-half of the actual 1.95-Hz oscillation frequency, is best appreciated when looping continuously and at maximum size. Half of the experiments were done with the camera in the landscape orientation and half were done in the portrait orientation. The plus-sign-shaped movie shown here is a composite, made by overlaying the landscape patterns on top of the portrait patterns. Because patterns are symmetrical around the center, a single quadrant contains all of the information. Therefore we present both active and relaxed, and high and low gain patterns in this composite movie as follows. Left half is from stretch-activated muscle; right half is from relaxed oscillations. Top half is high gain (all intensities multiplied by 20), which shows the weakest reflections at the expense of saturating the strong reflections; bottom half is low gain to show the strongest reflections. The major reflections analyzed in this work are labeled in yellow on the active side. Corresponding reflections in the relaxed half are symmetrically placed opposite the vertical dividing line. The reflections from the target zones (T-zone), tropomyosin (TM), myosin helix (M5 and M11), and actin helix (A6 and A7) are most easily seen in the top half, whereas the cross-bridge (CB) and troponin (Tn) reflections are most easily seen in the bottom half. On the active side, the tropomyosin and target zone reflections flash brighter while the cross-bridge and troponin reflections go dimmer as the muscle is stretched. In contrast, all four reflections remain relatively steady on the relaxed side. The A6 and A7 reflections on both sides of the pattern are moving up and down axially by a very small amount, as are the M5 and M11 reflections, although this movement is subtle and requires close examination. In the bottom corners, the average total force is plotted as a function of the fiber length. These form closed loops in which the area inside the loop represents the total work per cycle. In the active muscles, the loop is traversed counterclockwise, indicating that the muscle is actively generating work (~20 nJ/[fiber•cm]), whereas in the relaxed muscle the loop is traversed clockwise, indicating that the muscle is absorbing work from the system (~ – 4 nJ/[fiber•cm]). In both active and relaxed muscles the patterns appear to "breath" side to side. This indicates that the filament lattice is compressed (~1.7%) when the muscles are stretched.

Movie S1 (MOV)

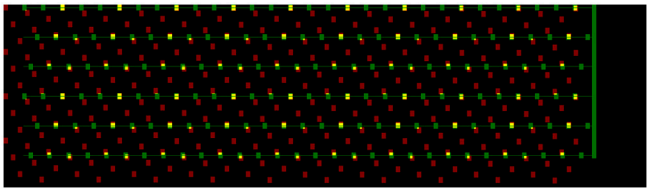

Movie 2. Dynamic matching of target zones and cross-bridges. In this 2D representation (radial projection), the 3D helical tracks of myosin heads on the surface of a half thick filament are shown as array of red rectangles that are arranged on diagonal lines. Each rectangle, 9 nm axially (horizontal) by 12° azimuthally (vertical), is the assumed range of motion for an individual myosin head (radial movements not considered here). The M band is at the left side of the movie. The myosin twist is visualized as a vertical lifting of the red cross-bridge array, most obvious at the right side of the movie. Superimposed on the red myosins are the relative locations of the target zones on the six surrounding thin filaments, shown as green rectangles (9 nm × 12°) connected by thin green lines. Target zones are moving back and forth due to the imposed 2.2% length oscillation. On the right, the vertical green bar represents the Z band. Bright yellow indicates where the target zones and cross-bridges overlap. These overlaps are counted and shown in Fig. 6*E*. The movie is best appreciated by setting the player to loop continuously and maximizing the size.

Movie S2 (MOV)